

Effects of hydraulic conductivity/strength anisotropy on the stability of stratified, poorly cemented rock slopes

Jia-Jyun Dong^{a,b,*}, Chia-Huei Tu^c, Wong-Ru Lee^d, Yun-Jia Jheng^a

^a Graduate Institute of Applied Geology, National Central University, No. 300, Jungda Rd., Jungli City 32001, Taiwan

^b Graduate Institute of Geophysics, National Central University, No. 300, Jungda Rd., Jungli City 32001, Taiwan

^c Department of Resources Engineering, National Cheng Kung University, No. 1, University Rd., Tainan City 70101, Taiwan

^d Geotechnical Engineering Research Center, Sinotech Engineering Consultants, Inc., Basement No. 7, Lane 26, Yat-Sen Rd., Taipei City 11071, Taiwan

ARTICLE INFO

Article history:

Received 5 December 2010

Received in revised form 1 November 2011

Accepted 1 November 2011

Keywords:

Stratified

Poorly cemented rock slopes

Hydraulic conductivity anisotropy

Strength anisotropy

Slope stability

ABSTRACT

This paper presents a numerical procedure to explore how hydraulic conductivity anisotropy and strength anisotropy affect the stability of stratified, poorly cemented rock slopes. The results provide information about the anisotropic characteristics of the medium, including the orientation of bedding planes, the anisotropic ratios of the hydraulic conductivity and the geological significance of the hydraulic conductivity anisotropy on the pore water pressure (PWP) estimation of finite slopes. Neglecting the hydraulic conductivity anisotropy of a slope with horizontal layers leads to a 40% overestimation of the safety factor. For a dip slope with inclined layers with $\theta = 30^\circ$, including the strength anisotropy caused a 25% reduction of the safety factor compared to the cases which isotropic strength is assumed. This paper highlights the importance of the hydraulic-conductivity anisotropy and the strength anisotropy on the stability of stratified, poorly cemented rock slopes.

© 2011 Elsevier Ltd. All rights reserved.

1. Introduction

Poorly cemented conglomerate, sandstone, siltstone, mudstone and shale are dominant formations distributed throughout the outer zone of the western foothills of Taiwan (hereafter outer foothill zone; the western portion of Taiwan's western foothills). Fig. 1 shows the location of the outer foothill zone. Gently warped Pliocene to Pleistocene sedimentary rocks crop out in these regions. Yen et al. [1] reported several slope failures triggered by heavy rainfall during the construction of a highway in northwestern Taiwan, an area in which rainfall triggered landslide is quite common. Among others, a multiple retrogressive landslide of the outer foothill zone near Hsin-Chu County in northwestern Taiwan is a typical case. There were nine events of slope movement be reported from 1935 to 1993 after heavy rainfall [2]. The failed slopes were composed of stratified, poorly cemented sandstone, siltstone, mudstone and shale with a dip angle of approximately 5° . A stream passes through the toe of the active landslide area. Springs on the surface of slopes indicate the presence of groundwater discharge.

Three features are critical for analyzing the groundwater flow and the stability of a slope composed of stratified and poorly

cemented rocks distributed in the northern portion of the outer foothill zone: (1) poorly cemented rocks are nearly soil-like; (2) joints are rarely observed in the field; and (3) stratified rocks are heterogeneous and anisotropic. These features are discussed in detail in the following section.

First, the uniaxial compressive strength of poorly cemented rocks distributed in the northern portion of the outer foothill zone is usually less than 5 MPa (as shown in Table 1 [3]). Usually, extremely weak materials are difficult to be sampled and tested. The representative strength of the soft rocks could be even lower than the value listed in Table 1. These rocks can be categorized from very weak to extremely weak [4]. Consequently, poorly cemented rocks are nearly soil-like.

Second, although it has been found that the structural features of the inner zone of Taiwan's western foothills (hereafter inner foothill zone; the eastern portion of Taiwan's western foothills) involve imbricate thrusting and asymmetric folding, contradistinctively, faulting is less prevalent and folds are fairly broad and gentle in the outer foothill zone [5]. Biq [6] suggested that the structural features of the outer foothill zone were produced in response to the impetus of allochthonous glide blocks that have come to rest on the inner foothill zone. As a result, the spacing of joints in most of the poorly cemented rocks is extremely wide (as shown in Fig. 2). Because the poorly cemented rocks are soil-like, the stressed joints in poorly cemented rocks would tend to be sealed. That is, the influence of joints on groundwater flow becomes less significant as the

* Corresponding author at: Graduate Institute of Applied Geology, National Central University, No. 300, Jungda Rd., Jungli City 32001, Taiwan. Tel./fax: +886 3 4224114.

E-mail address: jjdong@geog.ncu.edu.tw (J.-J. Dong).

Table 1

Uniaxial compressive strength of poorly cemented rocks distributed in the northern portion of the outer foothill zone [3].

Pleistocene	Yangmei formation	Toukoshan formation	Tananwan formation
Sandstone	3.40 MPa	3.10 MPa	0.39 MPa
Mudstone	2.80 MPa	2.60 MPa	(Siltstone)

depth gradually increases. Combining features (1) and (2) discussed above, the characteristics of groundwater flow in poorly cemented rock slopes are quite different from those in hard-jointed rock slopes where dominating types of groundwater flow are primarily conduit and fissure flows. For poorly cemented rocks, Huang et al. [7]

showed that the in situ hydraulic conductivity from Lugeion tests of sandstones in Hsin-Chu County was almost within the same order as that derived from laboratory tests. Similar results were also observed for Navajo sandstone [8]. Brace [9] concluded that fractures might play a minor hydrologic role for certain argillaceous rocks and sandstone. Consequently, it is reasonable to assume that the groundwater flow in poorly cemented rock slopes is likely dominated by intergranular flow. Hence, Darcy's law is valid.

Third, poorly cemented rocks in the northern portion of the outer foothill zone are stratified and therefore heterogeneous. Thin, alternating beds of shale, siltstone and sandstone are common in the northern portion of the outer foothill zone (as shown in Fig. 3). Table 2 shows some typical laboratory values of the measured hydraulic conductivities of Pliocene to Pleistocene

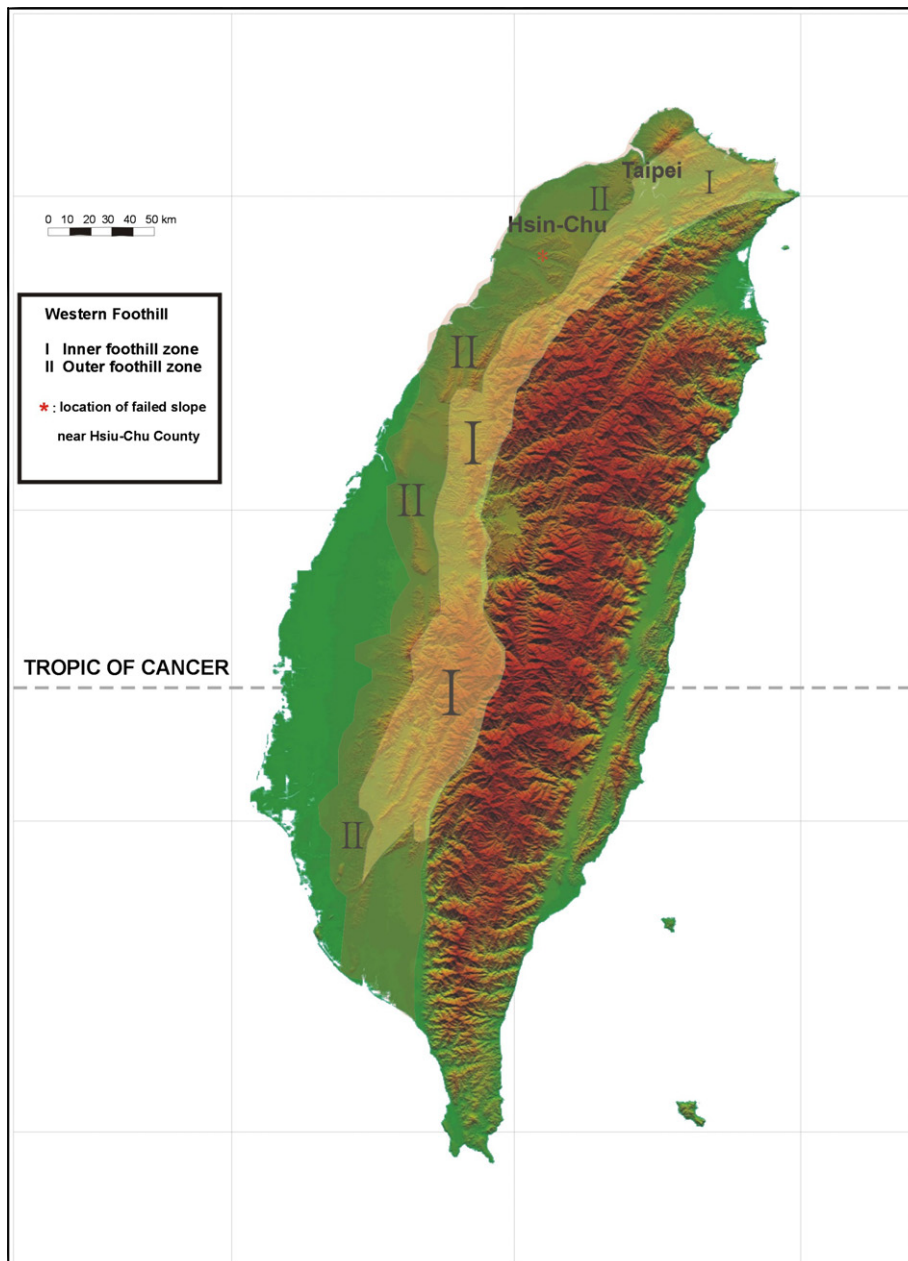


Fig. 1. Location of Taiwan's western foothills. The inner foothill zone and the outer foothill zone are the eastern portion and western portion of Taiwan's western foothills, respectively. Poorly cemented conglomerate, sandstone, siltstone, mudstone and shale are the dominant formations distributed throughout the northern portion of the outer foothill zone. Thick, massive mudstone crops out in the southern portion of the outer foothill zone.



Fig. 2. Poorly cemented rocks in the northern portion of the outer foothill zone. Massive sandstone crops out in an open cut near Hsin-Chu County, Taiwan. The imperceptible joints and uniform weathering condition indicate the groundwater in this region is likely dominated by intergranular flow.



Fig. 3. Poorly cemented, thin, alternating beds of shale and sandstone in the northern portion of the outer foothill zone.

sedimentary rocks distributed in northwestern Taiwan under steady flow conditions [10–12]. The hydraulic conductivity values of silty-shale to shaly-siltstone samples range from 10^{-6} to 10^{-11} cm/s. In comparison, hydraulic conductivity values of sandstones are generally higher, ranging from 10^{-3} to 10^{-9} cm/s.

To numerically analyze groundwater flow within a slope composed of stratified cemented rock, a dense mesh is required to determine the boundaries of each layer. However, this approach may become intractable and time-consuming when the slope is comprised of alternating beds with many extremely thin layers. When the heterogeneous medium can be replaced by a homogeneous medium with anisotropy by introducing a set of overall equivalent hydraulic conductivities, only a low-density mesh is required. Dong et al. [13] validated the notion of representing thin alternating beds of stratified, poorly cemented rocks as an equivalent anisotropic medium for groundwater flow analysis in finite slopes. Fig. 4 shows the equipotentials, flow lines and phreatic surfaces for the heterogeneous and equivalent anisotropic slopes. The stratified medium (in Fig. 4a) comprises several layers of two isotropic materials that have the same thickness ($t_I = t_{II} = 0.45$ m). The

Table 2

Typical values of the hydraulic conductivity of poorly cemented rocks distributed in the northern portion of the outer foothill zone [10–12].

Late Pleistocene to early Pliocene	Sandstone	Shaly-siltstone to silty-shale
Pan and Chen [10]	10^{-6} – 10^{-3} cm/s	–
Chen et al. [11]	10^{-9} – 10^{-5} cm/s	10^{-10} – 10^{-7} cm/s
Dong et al. [12]	10^{-5} – 10^{-4} cm/s	10^{-11} – 10^{-6} cm/s

hydraulic conductivities of these two materials are $k_I = 10^{-5}$ cm/s and $k_{II} = 10^{-7}$ cm/s, respectively. Theoretically, the equivalent hydraulic conductivities $(k_x)_{equi}$ and $(k_y)_{equi}$ in the principal directions of the stratified medium are directly derived [14] as follows:

$$(k_x)_{equi} = \frac{1}{(t_I + t_{II})} [k_I \cdot t_I + k_{II} \cdot t_{II}] \quad (1)$$

$$(k_y)_{equi} = \frac{(t_I + t_{II})}{\frac{t_I}{k_I} + \frac{t_{II}}{k_{II}}} \quad (2)$$

The hydraulic conductivities in principal directions of the equivalently homogenous anisotropic medium (Fig. 4b) are $(k_x)_{equi} = 5.05 \times 10^{-6}$ cm/s and $(k_y)_{equi} = 1.98 \times 10^{-7}$ cm/s. Based on Fig. 4, it is evidence that for thin, alternating beds of stratified, poorly cemented rock slope, ground water flow can be modeled using equivalently homogeneous, anisotropic hydraulic conductivity.

The effect of hydraulic conductivity anisotropy on the pore water pressure (PWP) distribution in a layered slope has been investigated [13]. Based on limited cases (three models with different hydraulic conductivity anisotropy), Dong et al. [13] demonstrated that the hydraulic conductivity anisotropy affects the safety factor and the critical sliding surface. In addition to considering the effect of hydraulic conductivity anisotropy on the slope stability [13,15], considering the influence of strength anisotropy on the slope stability analysis is also essential [16,17]. The mobilized shear strength along a failure surface would be expected to vary with the orientation of the failure plane because of both initial anisotropy and reorientation of the principal stress direction [18]. Schweiger et al. [19] proposed a multilaminate model to evaluate the safety factor of a slope composed of clay with strength anisotropy. With increasing strength anisotropy, the differences between the results of isotropic and anisotropic analyses become significant. Regarding the stability analysis of a slope composed of anisotropic soil, Al-Karni and Al-Shamrani [18] concluded that further research is required to better understand the coupled effects of strength anisotropy and PWP on slope stability.

Recognizing the hydro-mechanical coupled effects are complex, this study explores the uncoupled influence of hydraulic conductivity anisotropy and strength anisotropy on the slope stability of a stratified, poorly cemented rock slope via numerical experiments based on the work of Dong et al. [13]. First, the distribution of PWP in modeled slopes with hydraulic conductivity anisotropy (different anisotropic ratios of hydraulic conductivity and different dip angles of stratification) is calculated based on two-dimensional groundwater flow analysis [13]. Second, utilizing the limit equilibrium method, the safety factors and the failure planes of these finite slopes were calculated with isotropic strength parameters (cohesion c and friction angle ϕ). Finally, the anisotropic strength parameters were incorporated into the stability analysis, and the influence of hydraulic conductivity anisotropy and strength anisotropy on the slope stability of stratified and poorly cemented rock slopes was elucidated.

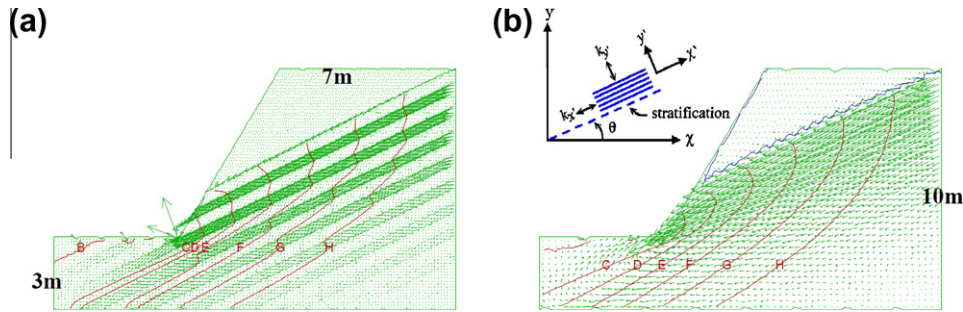


Fig. 4. The equipotentials, flow lines and phreatic surfaces for: (a) heterogeneous and (b) equivalent anisotropic slopes [13]. The dip angle of stratification θ (counterclockwise rotation from the global to local coordinates system x, y and x', y') is equal to 26.6° . Total head on equipotential lines C and H is 4 m and 9 m, respectively.

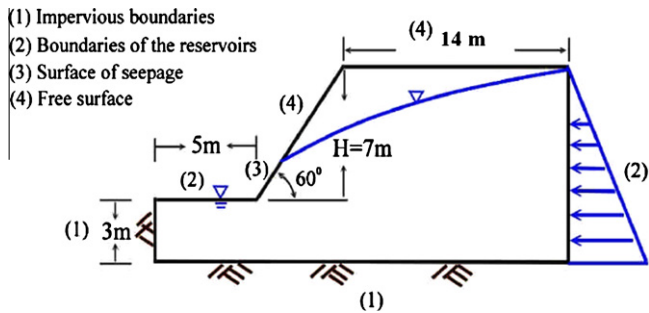


Fig. 5. Geometrical and boundary conditions for the modeled finite slope.

2. Research methods and numerical procedures

2.1. Creating the PWP contours

Two-dimensional, gravity-driven groundwater flow for an anisotropic finite slope can be simulated by the following expression for a local (x', y') coordinate system [20] (Fig. 4):

$$k_{x'} \frac{\partial^2 h}{\partial x'^2} + k_{y'} \frac{\partial^2 h}{\partial y'^2} = 0. \tag{3}$$

To create the PWP contours for analyzing the slope stability, an identical numerical tool – FLAC – adopted by Dong et al. [13] is used to calculate the PWP distributed in a 7-m-high finite slope with a 60° inclination. The geometry and boundary conditions of the modeled slope are shown in Fig. 5. The boundaries in the bottom and left are impermeable. The water table beyond the toe coincides with the ground surface indicating the modeled slope near a stream. A hydrostatic PWP distribution is applied on the right boundary of the proposed model and the total hydraulic head of the right vertical boundary is 10 m. The top flat surface is a free surface (no seepage occurs). The slope surface is a free surface or a surface of seepage.

Two indexes reflect the characteristics of anisotropy, namely the anisotropic ratios $k_{x'}/k_{y'}$ and the dip angles of stratification θ in the modeled slope. In the northern section of the Taiwan outer foothill zone, the dip angle of the poorly cemented rocks is generally less than 30° . From Table 2, the differences of the hydraulic conductivity values of silty-shale, shaly-siltstone and sandstone samples can be up to eight orders of magnitude. Fig. 6 shows that if the hydraulic conductivity ratio of the two alternating layers ranges from 10 to 10,000 (with low to medium hydraulic conductivity anisotropy), the equivalent hydraulic conductivity ratio $((k_{x'})_{equi}/(k_{y'})_{equi})$ is between 1 and 1000 with different thickness ratio (t_I/t_{II}) based on Eqs. (1) and (2). Accordingly, the modeled anisotropic ratios of the hydraulic conductivity $k_{x'}/k_{y'}$ are 10–1000. The

input properties for groundwater flow in all simulated cases are as follows: porosity = 0.3, density of water = 1000 kg/m^3 and bulk modulus of water = 10 kPa. A low bulk modulus of water is adopted to hasten the convergence of the calculation in these steady-state simulations.

Fig. 7 shows the calculated PWP distributed in the model slope with different anisotropic ratios $k_{x'}/k_{y'}$ and inclined angles of stratification θ . The selected principal values of the hydraulic conductivity tensor are (1) $k_{x'} = 10^{-5} \text{ cm/s}$ and $k_{y'} = 10^{-6} \text{ cm/s}$, (2) $k_{x'} = 10^{-5} \text{ cm/s}$ and $k_{y'} = 10^{-7} \text{ cm/s}$ and $k_{x'} = 10^{-5} \text{ cm/s}$ and $k_{y'} = 10^{-8} \text{ cm/s}$.

The related anisotropic ratios of the hydraulic conductivity $k_{x'}/k_{y'}$ are 10, 100 and 1000. The selected inclined angles θ between the maximum principal direction of the hydraulic conductivity tensor x' and the x -axis are 0° and $\pm 30^\circ$. A positive sign for θ denotes the simulated case of a dip slope where dip direction of stratification is in the same dip direction as the slope. A negative sign for θ indicates the simulated case of an anaclinal slope in

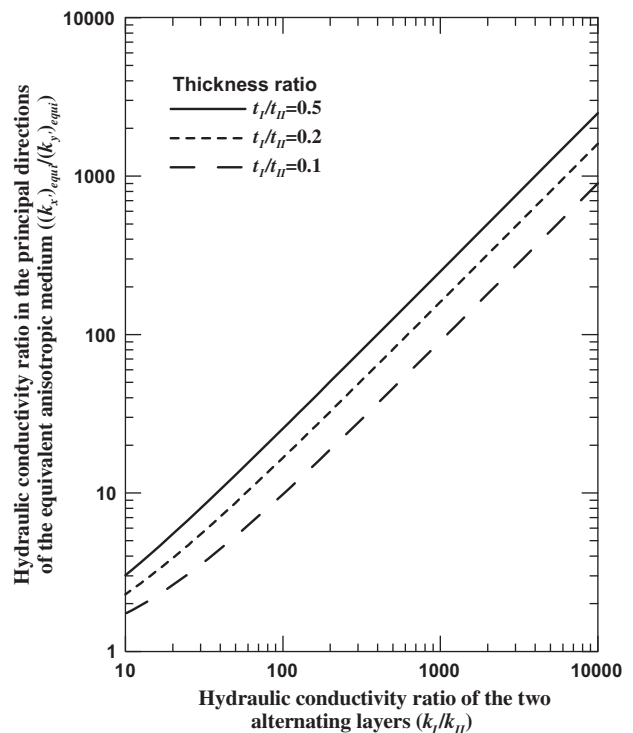


Fig. 6. The equivalent hydraulic conductivity ratio $((k_{x'})_{equi}/(k_{y'})_{equi})$ under different hydraulic conductivity ratio of the two alternating layers and different thickness ratio (t_I/t_{II}) .

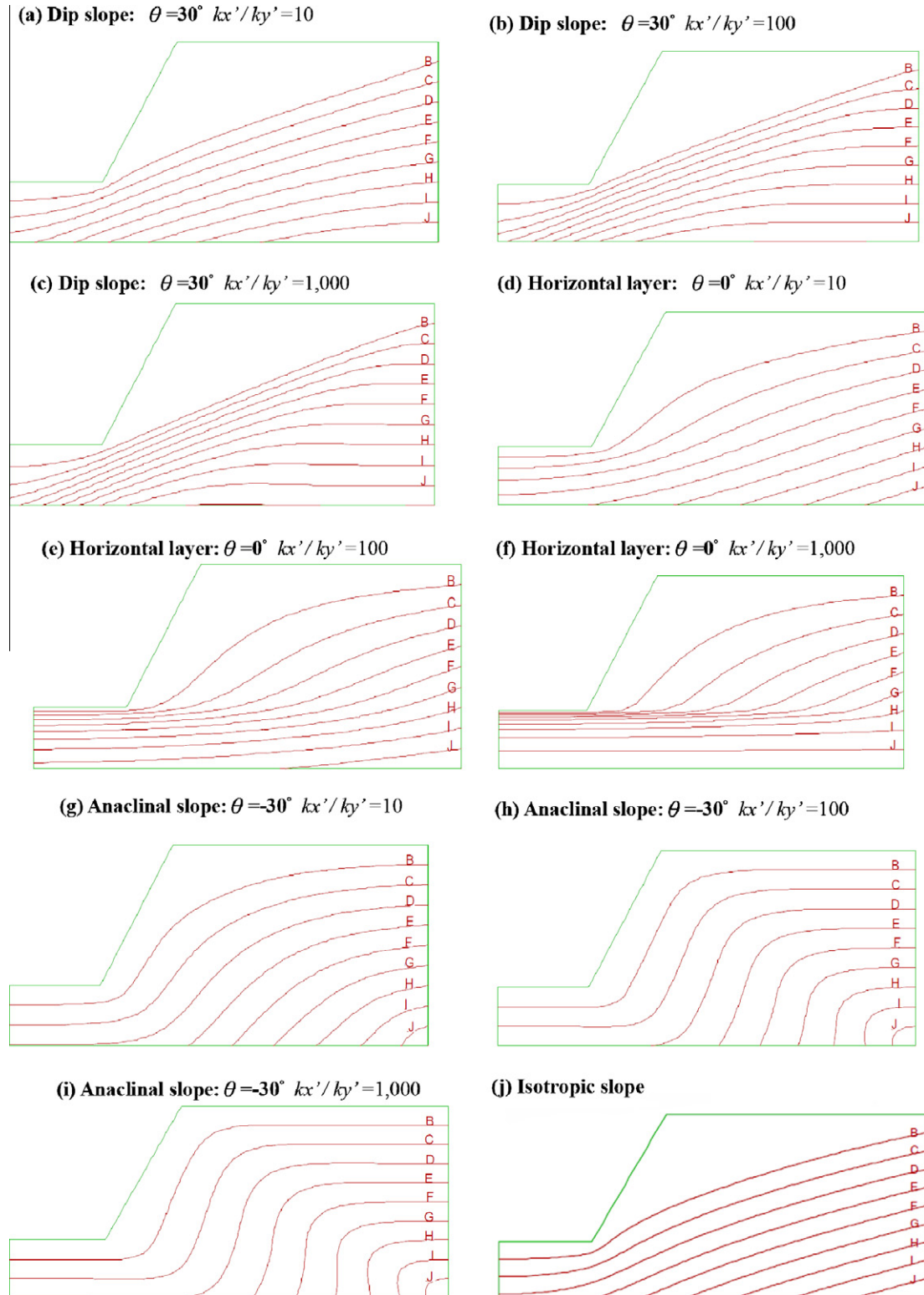


Fig. 7. Simulation results for groundwater flow in the modeled slopes. The PWP contours with labels B and J equal 10 kPa and 90 kPa, respectively.

which the dip direction of stratification is opposite to the dip direction of the slope. When $\theta = 0^\circ$, the stratified layer is horizontal. Based on the flow analysis results shown in Fig. 7, it can be digitalized into different pseudo layers with different PWPs. Accordingly, the influence of the hydraulic conductivity anisotropy could be considered in the slope stability analysis.

2.2. Slope stability analysis of stratified and poorly cemented rock slopes with strength anisotropy

The strength of stratified sedimentary rocks is anisotropic [21]. McLamore and Gray [22] showed that the maximum differential stress of Green River Shale is a function of the inclined angle between

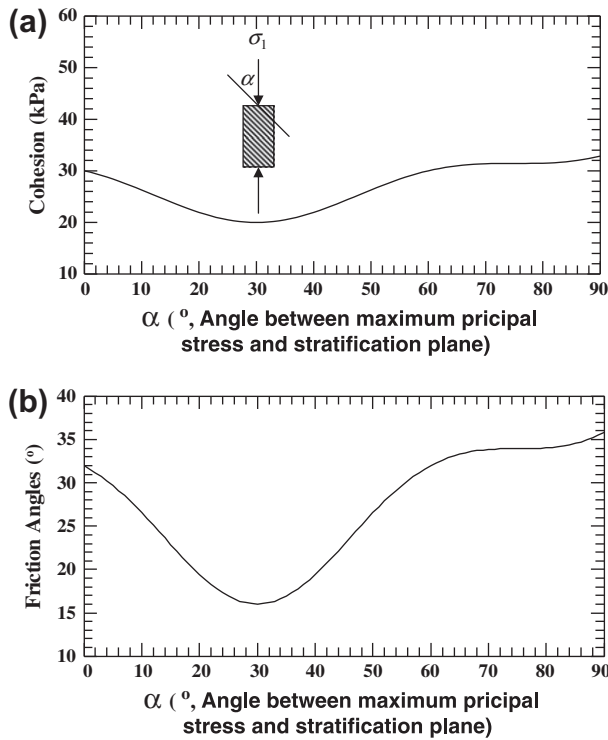


Fig. 8. The anisotropic strength parameters for different α . (a) Cohesion c (Eq. (6)); (b) friction angle ϕ (Eq. (7)).

the maximum principal stress and the bedding plane of the shale. If the Mohr–Coulomb failure criterion were adopted, the derived cohesion c and friction angle ϕ would be dependent on α (the angle between the maximum principal stress and the stratification plane).

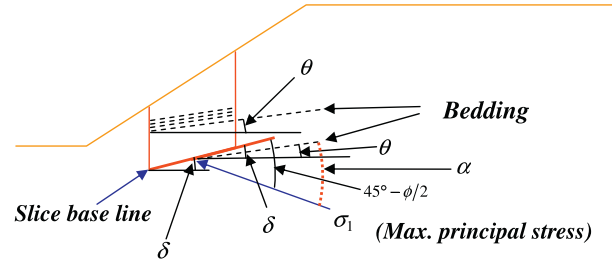


Fig. 9. Evaluating the angle α between the maximum principal stress and the bedding plane.

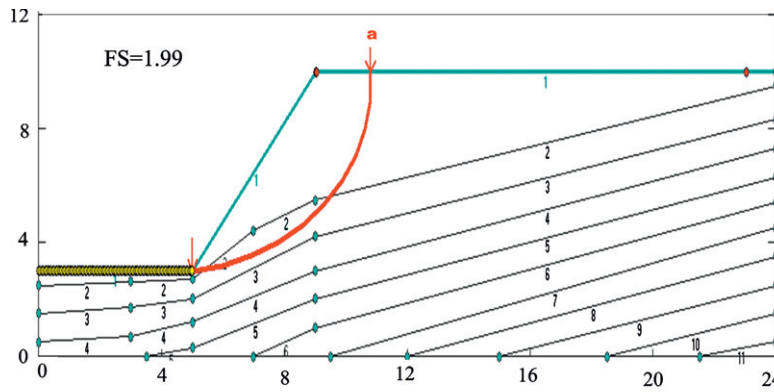
McLamore [23] proposed empirical functions to model the α dependent strength parameters as follows:

$$c = c_1 - c_2 \times [\cos(2 \times (\alpha - \alpha_{\min,c}))]^n \tag{4}$$

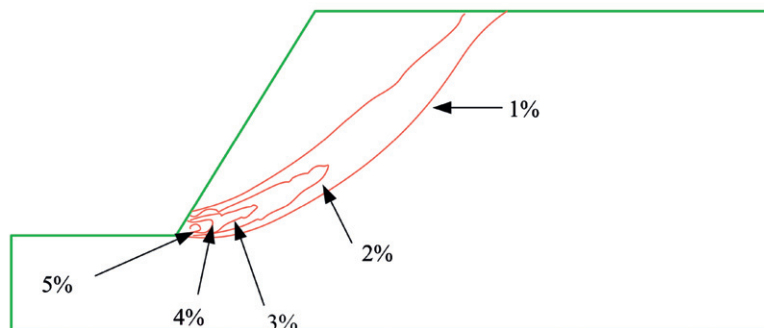
$$\tan \phi = \tan \phi_1 + (\tan \phi_2) \times [\cos(2 \times (\alpha - \alpha_{\min,\phi}))]^m, \tag{5}$$

where $c_1, c_2, \phi_1, \phi_2, m$ and n are material constants and $\alpha_{\min,c}$ and $\alpha_{\min,\phi}$ are the angle α where the lowest value of the strength parameters c and ϕ occurred. For example, $\alpha_{\min,c}$ and $\alpha_{\min,\phi}$ are 30° for the Green River Shale [22].

To consider the effect of strength anisotropy on the slope stability analysis, the McLamore's failure criterion [23] was used. The c and ϕ of the poorly cemented sedimentary sandstones are assumed as 30 kPa and 32° when the maximum principal stress is parallel to the bedding plane, i.e., $\alpha = 0^\circ$. This In addition, the lowest c and ϕ are assumed to be 20 kPa and 16° when $\alpha_{\min,c} = \alpha_{\min,\phi} = 30^\circ$ and $m = n = 3$. Accordingly, we assumed the anisotropic strength parameters to be defined as follows:



(a) The result of the slope stability analysis for a slope composed of an isotropic



(b) The safety factor for the modeled isotropic slope is 2.0 by Dong et al., [13].

Fig. 10. Variation of numerical result with the slope stability analysis for a slope composed of an isotropic medium.

$$c = 31.429 - 11.429 \times [\cos(2 \times (\alpha - 30^\circ))]^3; \tag{6}$$

$$\tan \phi = 0.673 - 0.386 \times [\cos(2 \times (\alpha - 30^\circ))]^3. \tag{7}$$

Based on Eqs. (6) and (7), the calculated c and ϕ for different α are shown in Fig. 8. Notably, the lowest c and ϕ ($\alpha = 30^\circ$) represent the strength parameters of the bedding planes. The highest c and ϕ ($\alpha = 90^\circ$) represent an uniaxial compression strength [24] of 0.13 MPa. For the modeled slopes with strength isotropy, $c = 30$ kPa and $\phi = 32^\circ$. The curves shown in Fig. 8 are a typical type for most of the stratified sedimentary rocks [25]. Ramamurthy [25] proposed a ratio of strength anisotropy R_c to evaluate the degree of strength anisotropy. The ratio of strength anisotropy could be expressed as follows:

$$R_c = \sigma_{c,90} / \sigma_{c,\min}, \tag{8}$$

where $\sigma_{c,90}$ is the uniaxial compression strength when the principal stress perpendicular to the bedding plane and $\sigma_{c,\min}$ are the lowest uniaxial compression strength of the rocks. For shale, the ratio of

strength anisotropy was $R_c = 1/4$. The parameters in Eqs. (6) and (7) we used represent a medium anisotropy with $R_c = 2$.

In this numerical procedure the limit equilibrium analysis program STABL5M [26] was adopted to analyze the slope stability. STABL5M program allows the users to input different c and ϕ in different directions when the “anisotropic soils” is selected. In this paper, we assumed that the maximum principal stress was inclined at an angle of $45^\circ - \phi/2$ to the slice base lines (Fig. 9). Given the stratification angle θ and the angle from the horizontal direction to the direction of slice base line δ (counterclockwise), the α between the stratification and the maximum principal stress of a specific slice base line could be calculated as follows:

$$\alpha = \left(45^\circ - \frac{\phi}{2}\right) - (\delta - \theta) \tag{9}$$

An iteration process is required for the friction angle ϕ is dependent on α . The lowest ϕ ($=16^\circ$) is assumed first. For a model slope with a given θ , the α of a slice base line with specific δ could be

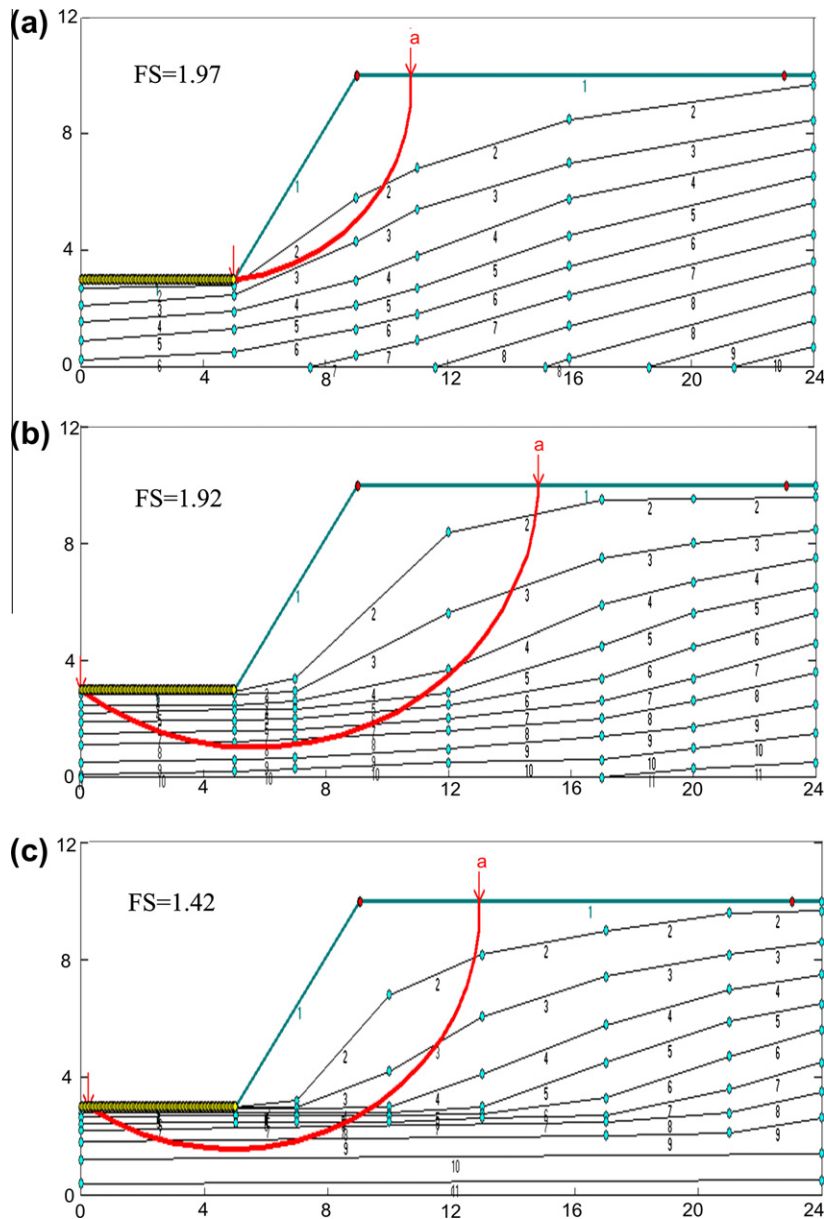


Fig. 11. The results of the slope stability analysis for a slope composed of an anisotropic medium with horizontal stratification layers. The anisotropic ratios of the hydraulic conductivity are 10, 100 and 1000 for (a) and (b), (c), respectively. The strength parameters are isotropic.

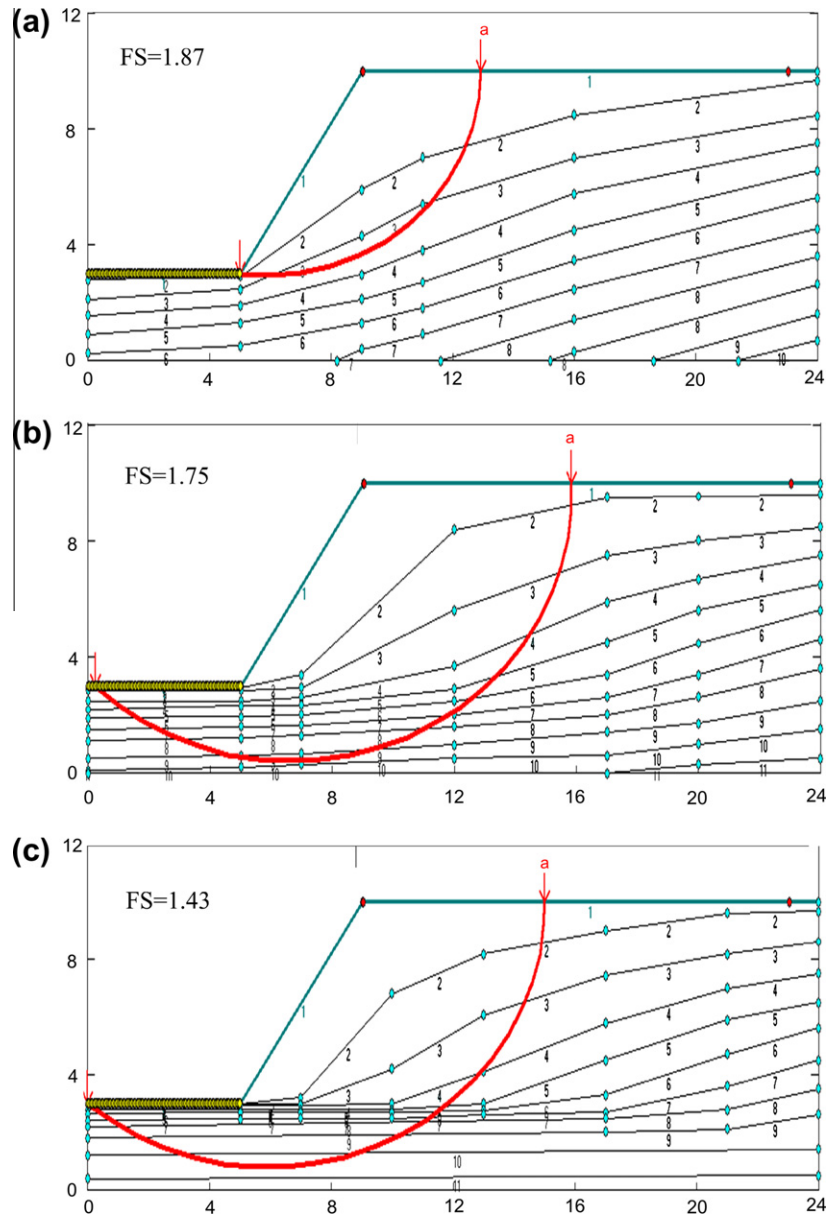


Fig. 12. The results of the slope stability analysis for a slope composed of an anisotropic medium with horizontal stratification layers. The anisotropic ratios of the hydraulic conductivity are 10, 100 and 1000 for (a) and (b), (c), respectively. The strength parameters are anisotropic.

determined using Eq. (9). Then a new ϕ can be determined using Eq. (7) and adopted to derive the new α . The iteration process converged quickly. Consequently, the c and ϕ of the anisotropic materials in different directions respective to the slice base line are obtained based on Eqs. (6) and (7). The different strength parameters c and ϕ are given counterclockwise from horizontal direction to the slice base line in 20° . As mentioned above, the poorly cemented rocks are soil-like. A circular failure mode was selected for analyzing the stability of the model slopes. The Bishop method was selected and the density of the medium was assumed to be 18.5 kN/m^3 .

3. Results of slope stability analysis

The numerical simulation results for anisotropic hydraulic conductivity/strength are analyzed with different PWP contours of the numerical models and strength parameters by the limit

equilibrium analysis program STABL5M. In this section, we compare the numerical results with the published literature to verify the proposed numerical procedures first. Then the results of slope stability analyses are demonstrated and discussed.

3.1. Definition of the observed factor

In order to evaluate the influences of hydraulic conductivity anisotropy and strength anisotropy on the slope stability of model slopes, two ratios are defined as follows:

$$Rk = \frac{FS_{ai}}{FS_{ii}} \quad (10)$$

$$Rs = \frac{FS_{aa}}{FS_{ai}} \quad (11)$$

where FS_{ii} , FS_{ai} , and FS_{aa} are the safety factors of the model slopes with isotropic hydraulic conductivity/strength, anisotropic hydraulic

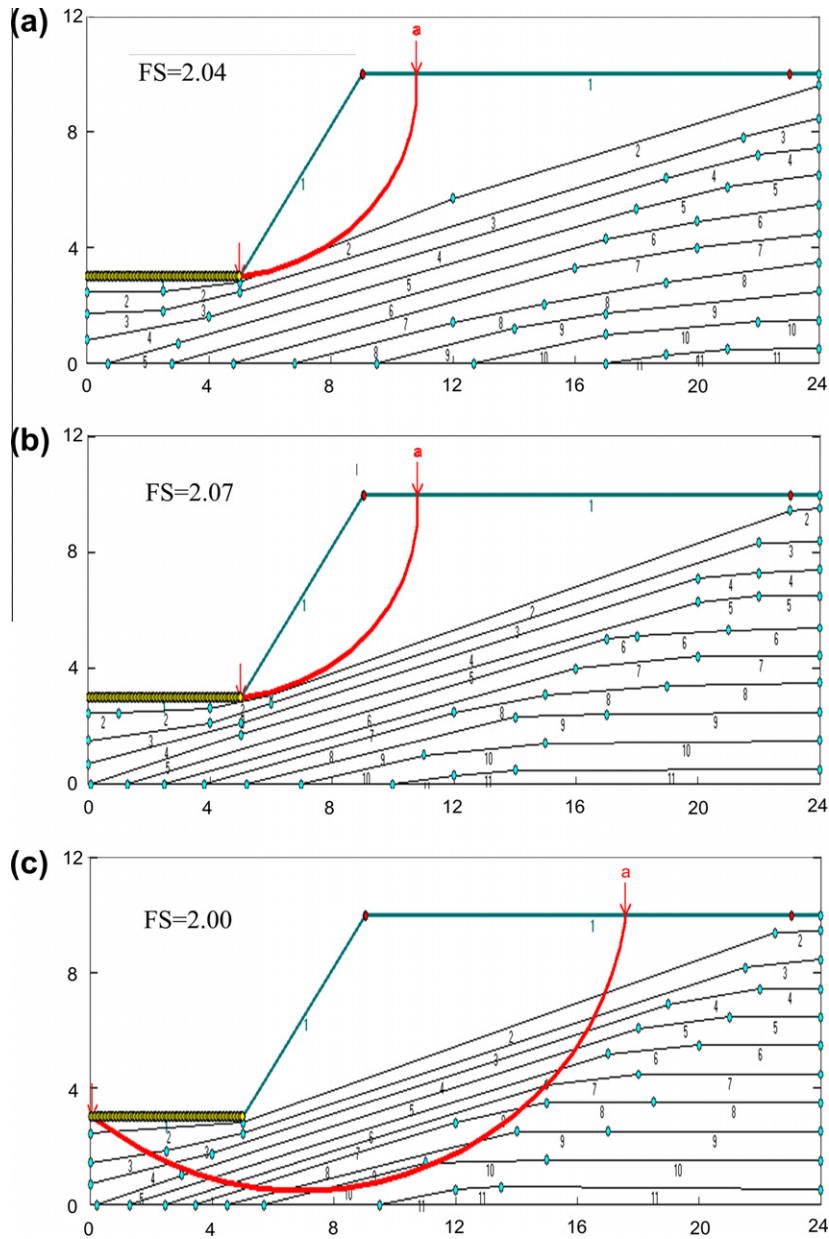


Fig. 13. The results of the slope stability analysis for a dip slope ($\theta = 30^\circ$) composed of an anisotropic medium. The anisotropic ratios of the hydraulic conductivity are 10, 100 and 1000 for (a) and (b), (c), respectively. The strength parameters are isotropic.

conductivity and isotropic strength and anisotropic hydraulic conductivity/strength, respectively. Accordingly, the ratios R_k and R_s indicate the influence of hydraulic conductivity anisotropy and strength anisotropy on the stability of the model slopes, respectively.

3.2. Verification of the numerical procedures

Fig. 10a shows the critical failure surface of a slope composed of an isotropic medium. The c and ϕ are 30 kPa and 32° ($\alpha = 0^\circ$), respectively. The pseudo layers in Fig. 10a for inputting different PWP's within the layers are digitalized from Fig. 7j. For example, the PWP between lines B and C is 15 kPa. An extrapolated layer with PWP value equals to 5 kPa is also provided. The calculated safety factor FS_{ii} equals to 1.99. Notably, the layers are only used for inputting different constant PWP's. The other parameters

(density, cohesion and friction angle) required in the analysis are identical for each layer. The critical failure surface and safety factor ($FS_{ii} = 2.0$) are almost identical to the simulation results using FLAC and a shear strength reduction technique [13], as shown in Fig. 10b.

3.3. Results of an anisotropic medium with anisotropic hydraulic conductivity

Figs. 11–16 show the results of slope stability analysis for the slopes composed of an anisotropic medium with anisotropic hydraulic conductivity. The slopes in Figs. 11–16 represent the slopes composed of horizontal layers, dip slopes with $\theta = 30^\circ$ and anaclinal slopes with $\theta = -30^\circ$, respectively. The anisotropic ratios of the hydraulic conductivity are 10, 100 and 1000 for (a), (b) and

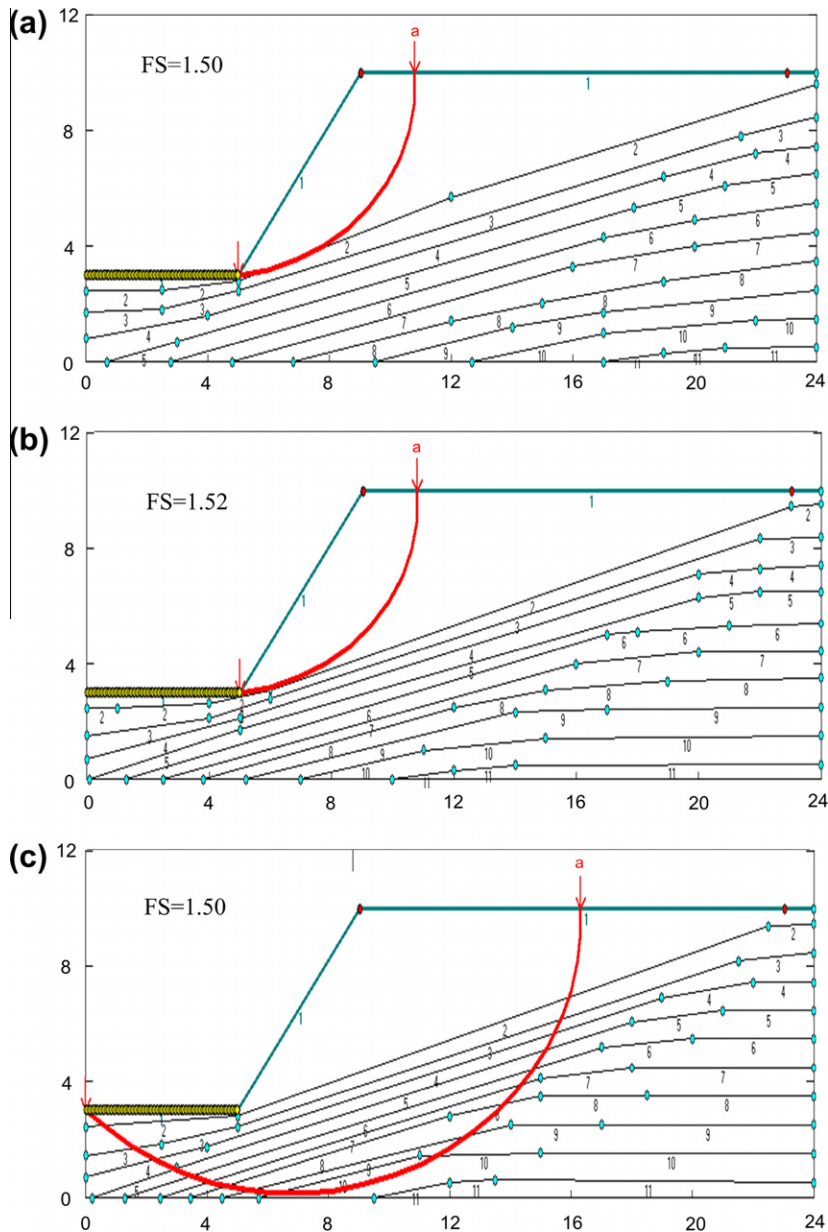


Fig. 14. The results of the slope stability analysis for a dip slope ($\theta = 30^\circ$) composed of an anisotropic medium. The anisotropic ratios of the hydraulic conductivity are 10, 100 and 1000 for (a) and (b), (c), respectively. The strength parameters are anisotropic.

(c), respectively. The strength parameters used in Figs. 11, 13 and 15 are isotropic, while the strength parameters used in Figs. 12, 14 and 16 are anisotropic (Eqs. (6) and (7)). The calculated safety factors (FS_{ai} and FS_{aa}) of all models are listed in Tables 3 and 4.

4. Discussion

4.1. Influence of hydraulic conductivity anisotropy on the slope stability of model slopes

Fig. 17 shows the influence of hydraulic conductivity anisotropy on the safety factor of the model slopes. Among the modeled slopes, the slope with horizontal layers ($\theta = 0^\circ$) has a lowest value of the Rk ($=0.71$) when $k_x/k_y = 1000$. This indicates that the safety factor of a slope with horizontal layers could be underestimated if the effect of the hydraulic conductivity anisotropy is neglected.

However, the influence of hydraulic conductivity is small when the slopes with $\theta = \pm 30^\circ$.

In addition, the critical failure surfaces of the slopes could also be affected by the hydraulic conductivity anisotropy. Two cases of modeled slopes with $\theta = 0^\circ$ ($k_x/k_y = 100, 1000$) and one case of model slope with $\theta = 30^\circ$ ($k_x/k_y = 1000$) (Figs. 11b, c and 13c) are significantly deeper than the ones with anaclinal slopes and the slope with isotropic hydraulic conductivity. Notably, the lines shown in Figs. 10–16 are digitization of the PWP distributions in Fig. 7. The induced error could be minimized if a software for slope stability analysis with ground water flow simulation is used.

4.2. Influence of the strength anisotropy on stability of model slopes

Fig. 18 shows the influence of the strength anisotropy on the safety factors (R_s) of the modeled slopes. As expected, the influence

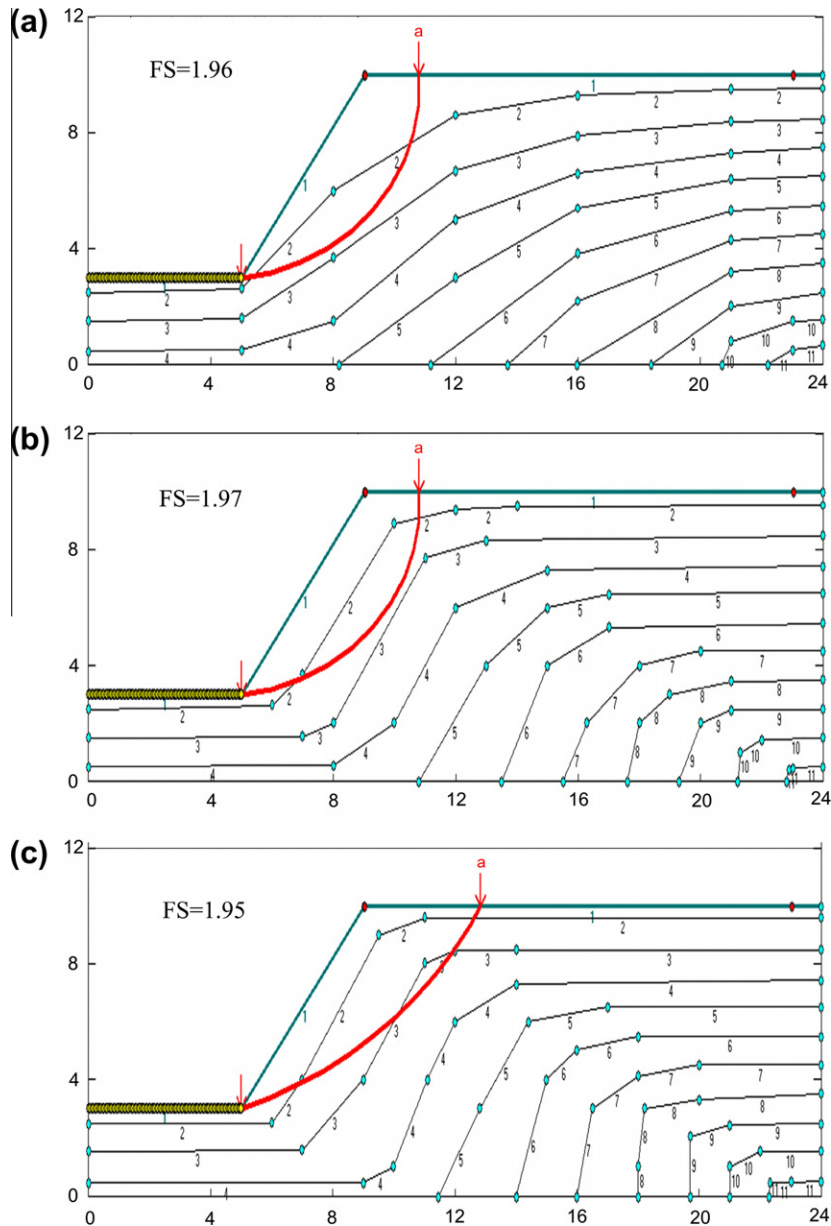


Fig. 15. The results of the slope stability analysis for an anacinal slope ($\theta = -30^\circ$) composed of an anisotropic medium. The anisotropic ratios of the hydraulic conductivity are 10, 100 and 1000 for (a) and (b), (c), respectively. The strength parameters are isotropic.

of strength anisotropy is most significant for the dip slopes. For the modeled dip slopes, the safety factors are reduced about 25% if the strength anisotropy is considered compared to the cases which isotropic strength is assumed (red¹ line in Fig. 18). Relatively, the influence of strength anisotropy is small for the slope with horizontal layers and anacinal slopes.

For anacinal slopes, the safety factors increased a small amount when the maximum principal stresses were nearly perpendicular to the stratification planes at some slice base lines. Accordingly, the c and ϕ increased a small amount compared with those cases with isotropic strength.

In general, the sliding surface depths of the anacinal slopes (Figs. 15 and 16) were shallow compared with the other examples (Figs. 11–14). In addition, the critical sliding surfaces of the slopes

with strength anisotropy are slightly deeper than those assumed the strength is isotropic (Figs. 11–16).

It is well known that the low strength of the bedding planes of a dip slope dominates the slope stability and that plane failures occur more frequently than circular failures. Notably, for a gentle dip slope composed of poorly cemented sedimentary rocks, even with flattened layers, the inherent anisotropy (including hydraulic conductivity and strength) also plays a very important role in its stability (blue lines in Figs. 17 and 18).

Finally, there is no attempt made to consider the coupled effect of hydraulic conductivity and strength on the stability a slope composed of stratified, poorly cemented rocks. Pan and Chen [10] suggested that the seepage-induced degradation might reduce the strength of soft rocks. Meanwhile, the stress-induced microcracks developed in a deformed slope could alter the hydraulic conductivity anisotropy of the soft rocks. Further research to consider these coupled effects of strength and hydraulic conductivity on the slope stability is required.

¹ For interpretation of color in Figs. 17 and 18, the reader is referred to the web version of this article.

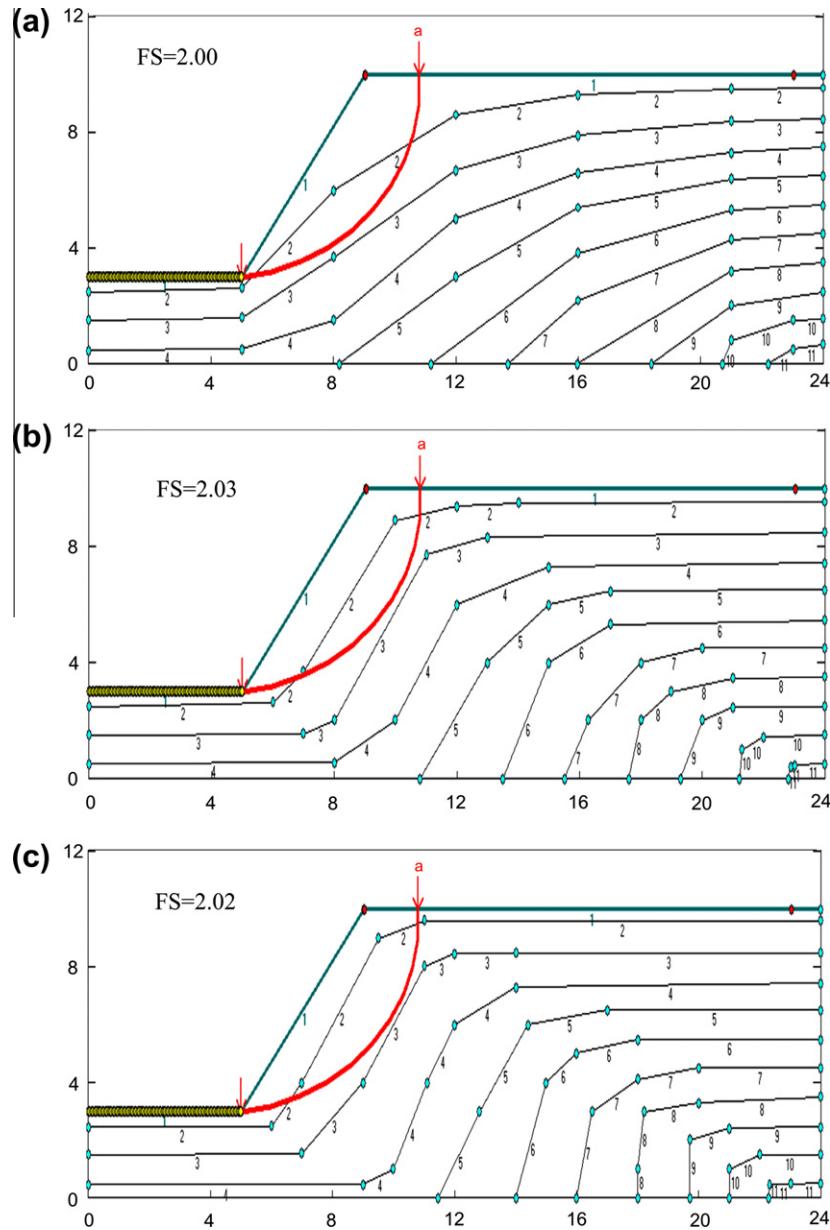


Fig. 16. The results of the slope stability analysis for an anaclinal slope ($\theta = -30^\circ$) composed of an anisotropic medium. The anisotropic ratios of the hydraulic conductivity are 10, 100 and 1000 for (a) and (b), (c), respectively. The strength parameters are anisotropic.

Table 3
Safety factors (FS_{ai}) of the slope with an anisotropic hydraulic conductivity when the strength parameters are isotropic.

	$k_x/k_y = 10$	$k_x/k_y = 100$	$k_x/k_y = 1000$
$\theta = 0^\circ$	1.97 (Fig. 11a)	1.92 (Fig. 11b)	1.42 (Fig. 11c)
$\theta = 30^\circ$	2.04 (Fig. 13a)	2.07 (Fig. 13b)	2.00 (Fig. 13c)
$\theta = -30^\circ$	1.96 (Fig. 15a)	1.97 (Fig. 15b)	1.95 (Fig. 15c)

Table 4
Safety factors (FS_{aa}) of the slope with an anisotropic hydraulic conductivity and anisotropic strength parameters.

	$k_x/k_y = 10$	$k_x/k_y = 100$	$k_x/k_y = 1000$
$\theta = 0^\circ$	1.87 (Fig. 12a)	1.75 (Fig. 12b)	1.43 (Fig. 12c)
$\theta = 30^\circ$	1.50 (Fig. 14a)	1.52 (Fig. 14b)	1.50 (Fig. 14c)
$\theta = -30^\circ$	2.00 (Fig. 16a)	2.03 (Fig. 16b)	2.02 (Fig. 16c)

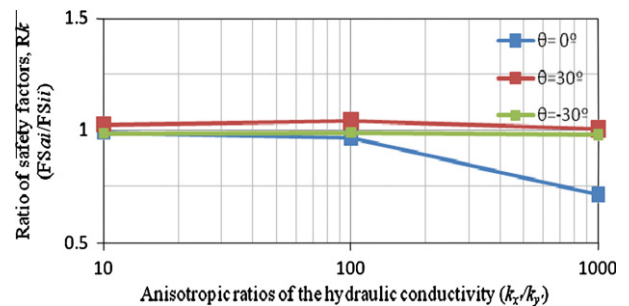


Fig. 17. The influence of the hydraulic conductivity anisotropy on the safety factors of the model slopes.

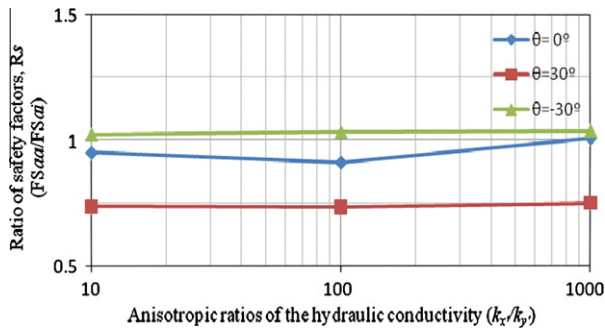


Fig. 18. The influence of strength anisotropy on the safety factors of the model slopes.

5. Conclusions

In this paper, we conducted a series of numerical experiments to study the impact of the anisotropic hydraulic conductivity/strength on the stability of slopes composed of poorly cemented sedimentary rocks. Based on the selected parameters which represent the hydro-mechanical characteristics of the poorly cemented rocks distributed in Taiwan, the following results were obtained:

1. The hydraulic conductivity anisotropy has significant impacts on the PWP distribution and stability of the model slopes with horizontal layers. The safety factor of an isotropic slope is 1.99. The safety factors of the slopes with horizontal layers decreased as the anisotropic ratio of the hydraulic conductivity increased. For the slope with horizontal layers, the safety factor was 1.42 when $k_x/k_y = 1000$. By neglecting the hydraulic conductivity anisotropy, the safety factor will be overestimated by 40% for the modeled cases.
2. The critical sliding surfaces are also dominated by the anisotropic characteristics of hydraulic conductivity. In general, the isotropic slope and anclinal slopes have shallow sliding surfaces compared with those of dip slopes and slopes with horizontal layers.
3. For a dip slope with inclined layers with $\theta = 30^\circ$, including the strength anisotropy caused a 25% reduction of the safety factor compared to the cases which isotropic strength is assumed.
4. Notably, a gentle dip slope composed of poorly cemented sedimentary rocks, even with flattened layers, the inherent anisotropy (including hydraulic conductivity and strength) plays an important role in its stability.
5. The critical sliding surfaces were not significantly changed when the strength anisotropy was considered.
6. To conclude, the geological structure play a dominate role on the slope stability of a rock slope composed of poorly cemented, layered sedimentary rocks, which reflected on the strength/hydraulic conductivity anisotropy. When evaluating the stability of slopes composed of poorly cemented, layered sedimentary rocks, the hydraulic conductivity anisotropy and the strength anisotropy should be taken into account.

Acknowledgements

The authors would like to thank the National Science Council of the Republic of China, Taiwan, for financially supporting this

research under Contracts Nos. NSC-99-2116-M-008-028 and NSC 100-3113-E-007-011. The authors also would like to thank two anonymous reviewers for their very constructive comments which greatly improved the manuscript.

References

- [1] Yen TL, Chen CH, Chin CT. Case histories of stabilization of highway slopes in soft sandstone and mudstone interbedded formation. *J Sino-Geotech* 1999;72:13–22 (in Chinese).
- [2] Lee WL. The investigation and analysis of Hu-Kou landslide [dissertation]. National Central University, Taiwan; 1994 (in Chinese).
- [3] Ku CS, Lee DH. Drilled shafts bearing capacity soft rock. *J Sino-Geotech* 2004;99:93–102 (in Chinese).
- [4] International Society for Rock Mechanics (ISRM), Commission on Classification of Rock and Rock Masses. Basic geotechnical description of rock mass. *Int J Rock Mech Mining Sci* 1981;18(1):85–110.
- [5] Ho CS. An introduction to the geology of Taiwan explanatory text of the geologic map of Taiwan. 2nd ed. Taiwan: Central Geological Survey; 1988.
- [6] Biq C. Dual-trench structure in the Taiwan-Luzon region. *Proc Geol Soc China* 1972;15:65–75.
- [7] Huang AB, Liao JJ, Pan YW, Cheng MH, Hsieh SY, Peng JK. Characterization of soft rocks in Taiwan. In: Girard J, Liebman M, Breeds C, Doe T, editors. *Pacific rocks 2000; rock around the rim: proceedings of the 4th North American rock mechanics symposium*; 2000 July 31–August 3, Seattle, Washington, USA. Rotterdam: AA Balkema; 2000. p. 83–90.
- [8] Nelson RA, Handin J. Experimental study of fracture permeability in porous rock. *Am Assoc Petrol Geol Bull* 1977;61:227–36.
- [9] Brace WF. Permeability of crystalline and argillaceous rocks. *Int J Rock Mech Mining Sci* 1980;17:241–51.
- [10] Pan YW, Chen HY. A permeability apparatus and seepage induced degradation of soft rock. *J Geotech* 2009;4:51–62.
- [11] Chen TMN, Zhu W, Wong TF, Song SR. Laboratory characterization of permeability and its anisotropy of Chelungpu fault rocks. *Pure Appl Geophys* 2009;166:1011–36.
- [12] Dong JJ, Hsu JY, Wu WJ, Shimamoto T, Hung JH, Yeh EC, et al. Stress-dependence of the permeability and porosity of sandstone and shale from TCDP Hole-A. *Int J Rock Mech Mining Sci* 2010;47:1141–57.
- [13] Dong JJ, Tzeng JH, Wu PK, Lin ML. Effects of anisotropic permeability on stabilization and pore water pressure distribution of poorly cemented stratified rock slopes. *Int J Numer Anal Methods Geomech* 2006;30:1579–600.
- [14] Terzaghi K, Peck RB, Mesri G. *Soil mechanics in engineering practice*. New York: John Wiley & Sons Inc; 1996.
- [15] Ng CWW, Shi Q. A numerical investigation of the stability of unsaturated soil slopes subjected to transient seepage. *Comput Geotech* 1998;22(1):1–28.
- [16] Hwang J, Dewoolkar M, Ko HY. Stability analysis of two-dimensional excavated slopes considering strength anisotropy. *Can Geotech J* 2002;39(5):1026–38.
- [17] Shogaki T, Kumagai N. A slope stability analysis considering undrained strength anisotropy of natural clay deposits. *Soils Found* 2008;48:805–19.
- [18] Al-Karni AA, Al-Shamrani MA. Study of the effect of soil anisotropy on slope stability using method of slices. *Comput Geotech* 2000;26:83–103.
- [19] Schweiger HF, Wiltafsky C, Scharinger F, Galavi V. A multilaminate framework for modelling induced and inherent anisotropy of soils. *Geotechnique* 2009;59(2):87–101.
- [20] Zienkiewicz OC, Mayer P, Cheung YK. Solution of anisotropic seepage by finite elements. *J Eng Mech, ASCE* 1966;92:111–20.
- [21] Chenevert ME, Gatlin C. Mechanical anisotropies of laminated sedimentary rocks. *J Soc Petrol Eng* 1965;5:67–77.
- [22] McLamore RT, Gray KE. The mechanical behavior of anisotropic sedimentary rocks. *J Eng Ind Res* 1967;89:62–76.
- [23] McLamore RT. Strength-deformation characteristic of anisotropic sedimentary rocks [dissertation]. University of Texas, Austin, USA; 1966.
- [24] Goodman RE. *Introduction to rock mechanics*. 2nd ed. John Wiley & Sons; 1989.
- [25] Ramamurthy T. Strength and modulus responses of anisotropic rocks. In: Brown ET, editor. *Comprehensive rock engineering: principles, practice & projects. Fundamentals*, vol. 1. Oxford, New York: Pergamon Press; 1993. p. 313–9.
- [26] Achilleos, E. User guide for PCSTABL5M. Joint highway research rep. no. JHRP-88/19, Purdue Univ., West Lafayette, In, USA; 1988.